

AN EMPIRICAL RELATION BETWEEN THE LARGE-SCALE MAGNETIC FIELD AND THE DYNAMICAL MASS IN GALAXIES

F. S. Tabatabaei, T. P. K. Martinsson, J. H. Knapen, J. E. Beckman¹

Instituto de Astrofísica de Canarias, Vía Láctea S/N, E-38205 La Laguna, Spain

Departamento de Astrofísica, Universidad de La Laguna, E-38206 La Laguna, Spain

ftaba@iac.es

B. Koribalski

CSIRO Astronomy and Space Science, Australia Telescope National Facility, Epping, NSW

1710, Australia

and

B. G. Elmegreen

IBM T. J. Watson Research Center, 1101 Kitchawan Road, Yorktown Heights, NY 10598,

USA

Received _____; accepted _____

¹Consejo Superior de Investigaciones Científicas

ABSTRACT

The origin and evolution of cosmic magnetic fields as well as the influence of the magnetic fields on the evolution of galaxies are unknown. Though not without challenges, the dynamo theory can explain the large-scale coherent magnetic fields which govern galaxies, but observational evidence for the theory is so far very scarce. Putting together the available data of non-interacting, non-cluster galaxies with known large-scale magnetic fields, we find a tight correlation between the integrated polarized flux density, S_{PI} , and the rotation speed, v_{rot} , of galaxies. This leads to an almost linear correlation between the large-scale magnetic field \bar{B} and v_{rot} , assuming that the number of cosmic ray electrons is proportional to the star formation rate, and a super-linear correlation assuming equipartition between magnetic fields and cosmic rays. This correlation cannot be attributed to an active linear α - Ω dynamo, as no correlation holds with global shear or angular speed. It indicates instead a coupling between the large-scale magnetic field and the dynamical mass of the galaxies, $\bar{B} \sim M_{\text{dyn}}^{0.25-0.4}$. Hence, faster rotating and/or more massive galaxies have stronger large-scale magnetic fields. The observed $\bar{B} - v_{\text{rot}}$ correlation shows that the anisotropic turbulent magnetic field dominates \bar{B} in fast rotating galaxies as the turbulent magnetic field, coupled with gas, is enhanced and ordered due to the strong gas compression and/or local shear in these systems. This study supports an stationary condition for the large-scale magnetic field as long as the dynamical mass of galaxies is constant.

Subject headings: galaxies: general — galaxies: magnetic field — galaxies: star formation

1. INTRODUCTION

Magnetic fields are present on all scales in the universe from planets and stars to galaxies and galaxy clusters, and even at high redshifts. They are important for the continuation of life on the Earth, the onset of star formation, the order of the interstellar medium, and the evolution of galaxies (Beck & Wiełebinski 2013). Hence, understanding the Universe without understanding magnetic fields is impossible.

The most widely accepted theory to explain the magnetic fields on stars and planets is the dynamo theory. This describes the process through which a rotating, convecting, and electrically conducting fluid can maintain a magnetic field over astronomical timescales (Steenbeck & Krause 1969). A similar process can also explain the large-scale coherent magnetic fields in galaxies (see Widrow et al. 2002, and references therein). It is assumed that such fields arise from the combined action of helical turbulence and differential rotation, a process known as the α - Ω dynamo. While a number of fundamental questions concerning the nature of the galactic dynamo remain unanswered, so far no observational evidence for the effect of galaxy rotation on the large-scale magnetic field has been found. This motivated our currently reported investigation of a possible connection between the tracers of the large-scale magnetic field strength and the rotation of galaxies. Finding such a correlation observationally is not necessarily straightforward due to the possible dilution by galaxy-galaxy interactions and environmental effects which influence the rotation curves and possibly the magnetic fields. Such disturbing effects had to be taken into account when selecting the sample.

The present study is based on a careful measurement of the galaxy rotation speed as well as the model-free tracer of the large-scale magnetic field strength, the integrated polarized flux density (S_{PI}). We introduce the sample and the data in Sect. 2, and describe the v_{rot} measurements in Sect. 3. We investigate the possible correlations in Sect. 4 and

discuss and summarize the results in Sect. 5 and 6, respectively.

2. GALAXY SAMPLE

Not many galaxies are found in the literature with known polarized intensity measurements. Table 1 shows the 4.8 GHz integrated polarized intensity measurements for a sample of nearby galaxies, including Local Group galaxies and barred galaxies from Beck et al. (2002). To minimize environmental effects, we excluded galaxies in the Virgo and Ursa Major clusters, and those known to be in interacting systems. Measurements with poor signal-to-noise ratio (≤ 1) were also omitted. We included the Local Group dwarf galaxies from Chyży et al. (2011), as they also show large-scale coherent magnetic fields. Galaxies which fit our selection limits, i.e., with known large-scale magnetic fields and minimum environmental disturbances are listed in Table 1. Each galaxy was observed in polarized light at a linear resolution d smaller than the galaxy optical size (in the sample, $d < 0.25 \times R_{25}$, with R_{25} the optical radius). Thus, the large-scale magnetic field with a coherent length l (\simeq half a galaxy size, e.g., Fletcher 2010) is resolved in all galaxies and the beamwidth depolarization is small ($\sim d^2/l^2 \leq 6\%$ in the sample).

3. GALAXY ROTATION SPEEDS

The adopted rotation speed v_{rot} of the sample galaxies was derived in one of three ways, namely by I) averaging the rotation speed over the flat part of the rotation curves, II) using the corrected W_{20} measurements of HIPASS data, or III) taking values directly from the literature.

In case I, 10 galaxies had rotation curves derived by Sofue et al. (1999)¹; these are indicated with ‘S’ in Table 1. The measurements in the ‘flat part’ of the rotation curve were averaged to calculate v_{rot} (see the radial range for individual galaxies in Table 1). The errors were estimated assuming 10 km/s measurement errors (Sofue et al. 1997) and 3 degree errors on the inclination. Five galaxies (with reference indicators ‘A’, ‘B’, ‘BA’, ‘C’, ‘CS’) were taken from other papers (see references in Table 1). For the SMC, v_{rot} was derived by a weighted average in the flat part of the rotation curve presented in Bekki & Stanimirović (2009), assuming uncertainties of 6 km/s in velocity and 5 degrees in inclination. For NGC 3359, in a similar way, we read the 13 outer data points of the rotation curve in Figure 11 of Ball (1983), excluding the outermost point. For the remaining three galaxies, v_{rot} was calculated in the same way, but with measurements and errors given in their reference papers.

In case II, we derived v_{rot} from HI W_{20} measurements for eight galaxies (indicated by ‘W’ in Table 1). The W_{20} measurements were taken from Koribalski et al. (2004) and have been corrected for instrumental effects, internal turbulent motion and inclination following Martinsson et al. (2015), assuming a gas velocity dispersion $\sigma_{\text{HI}} = 10$ km/s and using the HIPASS spectral resolution of 18 km/s. The measurement errors on W_{20} were estimated to be three times the error on the systemic velocity as suggested by Koribalski et al. (2004), and the error on inclination was assumed to be three degrees for all galaxies.

For three galaxies, v_{rot} is taken from the literature (Mateo 1998, with superscript ‘M’ in Table 1), only correcting for the inclination (case III).

¹<http://www.ioa.s.u-tokyo.ac.jp/~sofue/RC99/rc99.htm>

4. A TIGHT CORRELATION

The polarized intensity (PI) provides a measure of the large-scale magnetic field in galaxies. It is defined through the integral over the path length L in the emitting medium

$$\text{PI} = K \int_L n_{\text{cr}} \bar{B}^2 dl, \quad (1)$$

with n_{cr} the cosmic ray electron number density, \bar{B} the large-scale transverse magnetic field strength averaged over the line of sight, and K a dimensional constant (Beck et al. 2003). The above definition is similar to that of the total intensity of the radio continuum emission,

$$I = K \int_L n_{\text{cr}} B^2 dl, \quad (2)$$

with B the total transverse magnetic field strength which includes both the large-scale uniform field and the local turbulent field, $\langle B^2 \rangle = \bar{B}^2 + \langle b^2 \rangle$, where $\langle b \rangle$ is the turbulent magnetic field strength. Observationally, the total intensity I is just a measure of the Stokes I parameter, while the linearly polarized intensity PI is a measure of the Stokes Q and U parameters,

$$\text{PI} = \sqrt{Q^2 + U^2}. \quad (3)$$

The integrated flux densities of the total intensity S_I and linearly polarized intensity S_{PI} (in units of Jansky) are obtained by integrating the I and PI maps (in Jansky/beam) over the area A ,

$$S_{\text{PI}} = \int \text{PI} \, dA = K \int \int_L n_{\text{cr}} \bar{B}^2 \, dl \, dA, \quad (4)$$

$$S_{\text{I}} = \int I \, dA = K \int \int_L n_{\text{cr}} B^2 \, dl \, dA. \quad (5)$$

For the selected sample of 26 galaxies, we collected S_{I} and S_{PI} at 4.8 GHz from the literature. Table 1 shows those fluxes, projected to a common distance of 10 Mpc. Plotting S_{PI} vs. v_{rot} we find a tight correlation (Fig. 1). The Pearson correlation coefficient is $r_{\text{p}} = 0.94 \pm 0.04$, and the Spearman rank coefficient $r_{\text{sp}} = 0.8 \pm 0.0$. The correlation is even tighter than that between S_{I} and v_{rot} with a rank $r_{\text{sp}} = 0.7 \pm 0.0$ (same figure). A linear fit in logarithmic plane leads to a slope of 4.6 ± 0.3 , slightly steeper than that found between S_{I} and v_{rot} (4.0 ± 0.3). The ratio of the integrated polarized to total flux density, $S_{\text{PI}}/S_{\text{I}}$, is not constant and increases with v_{rot} with a least square fit slope of 0.6 ± 0.2 and a bisector fit slope of 1.2 ± 0.3 .

5. DISCUSSION

Taking into account the well-known correlation between the total star formation rate (SFR) and radio luminosity of galaxies (Condon 1992) and the correlation between SFR and stellar mass (e.g. Sparre et al. 1998) which scales with v_{rot} according to the Tully-Fisher relation (Tully & Fisher 1977), are the observed correlations $S_{\text{I}} - v_{\text{rot}}$ and $S_{\text{PI}} - v_{\text{rot}}$ (Fig. 1) merely secondary correlations which represent a more direct relation between SFR and v_{rot} ? We estimated SFR by combining the GALEX far-UV (FUV) (Lee et al. 2011; Cotrese et al. 2012) and the IRAS $25\mu\text{m}$ fluxes (Abrahamyan et al. 2015) and following the calibration relation given by Hao et al. (2011) and Kennicutt et al. (2009):

$$\frac{\text{SFR}}{\text{M}_{\odot} \text{ yr}^{-1}} = 10^{-43.35} \left[\frac{\nu L_{\nu}(\text{FUV})}{\text{erg s}^{-1}} + 3.89 \times \frac{\nu L_{\nu}(25\mu\text{m})}{\text{erg s}^{-1}} \right]$$

In a few cases with no GALEX data, only the IR data were used to estimate the SFR following Kennicutt & Evans (2012):

$$\frac{\text{SFR}}{\text{M}_{\odot} \text{ yr}^{-1}} = 10^{-42.69} \frac{\nu L_{\nu}(24\mu\text{m})}{\text{erg s}^{-1}}.$$

Table 1 lists the SFR values obtained. We address the question raised by comparing the correlations of S_{I} and S_{PI} with SFR and v_{rot} . We found that indeed SFR is correlated with v_{rot} with $r_{\text{sp}} = 0.67$, similar to the $S_{\text{I}} - v_{\text{rot}}$ correlation ($r_{\text{sp}} = 0.72$), indicating that the SFR could be the main cause of the observed $S_{\text{I}} - v_{\text{rot}}$ correlation. This is shown better by a tighter correlation of S_{I} with SFR ($r_{\text{sp}} \sim 0.9$) than v_{rot} ($r_{\text{sp}} \sim 0.7$, Fig. 2).

The SFR – v_{rot} correlation is, however, not as tight as the $S_{\text{PI}} - v_{\text{rot}}$ correlation ($r_{\text{sp}} = 0.80$). Hence, the correlation between SFR and S_{PI} (Fig. 2) may not fully explain the tighter $S_{\text{PI}} - v_{\text{rot}}$ correlation. A correlation is expected between the integrated polarized flux density S_{PI} and SFR due to cosmic rays as their number N_{cr} increases with star formation activity (e.g. Murphy et al. 2008). Otherwise, no correlation is expected between the large-scale field \bar{B} (traced by PI) and SFR, while the turbulent (and total) magnetic field positively correlate with SFR (Tabatabaei et al. 2013a,b). This could also explain that the $S_{\text{I}} - \text{SFR}$ correlation is tighter than the $S_{\text{PI}} - \text{SFR}$ correlation (Fig. 2). We note that SFR is not a directly measured quantity. Potential systematic effects in calibration, like a dependence of the calibration factors on the galaxy properties, could increase uncertainties in SFR.

5.1. The Large-Scale Magnetic Field

Equation (4) can be written as $S_{\text{PI}} \sim \langle n_{\text{cr}} \rangle \bar{B}^2 V$, with V the integration volume. The ratio $S_{\text{PI}}/\langle n_{\text{cr}} \rangle$ is a measure of the energy of the large-scale magnetic field, $E(\bar{B}) = \bar{B}^2 V/8\pi$. Studying the corresponding energy density and the large-scale magnetic field strength is

then possible via $S_{\text{PI}}/N_{\text{cr}} \sim \bar{B}^2$ with $N_{\text{cr}} = \langle n_{\text{cr}} \rangle V$. The SFR can be taken as a proxy for N_{cr} (Sect. 5), and hence $S_{\text{PI}}/\text{SFR} \sim \bar{B}^2$. Fig. 3-top shows that S_{PI}/SFR is correlated with $v_{\text{rot}}^{1.8 \pm 0.3}$ with $r_{\text{p}} = 0.8 \pm 0.1$ and $r_{\text{sp}} = 0.7 \pm 0.0$. Thus, $\bar{B}^2 \sim S_{\text{PI}}/\text{SFR} \sim v_{\text{rot}}^2$ or $\bar{B} \sim v_{\text{rot}}$, the large-scale ordered field is linearly proportional to the rotation speed of the galaxies.

The relation between N_{cr} and SFR differs if an equipartition between the energy densities of the cosmic ray electrons and the total magnetic field holds. The global equipartition condition leads to $N_{\text{cr}} \sim B^2$, with B the mean total magnetic field strength in each galaxy. Independent observations show a global correlation between B and SFR in galaxies, $B \sim \text{SFR}^{0.25-0.3}$ (Chyży et al. 2011; Heesen et al. 2013). Thus, N_{cr} changes with SFR as $N_{\text{cr}} \sim \text{SFR}^{0.5-0.6}$. It then follows that $\bar{B}^2 \sim S_{\text{PI}}/N_{\text{cr}} \sim S_{\text{PI}}/\text{SFR}^{(0.5-0.6)}$, which is correlated to $\sim v_{\text{rot}}^{3.0 \pm 0.3}$ with $r_{\text{p}} = 0.9 \pm 0.1$ (Fig. 3-middle). Hence, a super-linear correlation holds between \bar{B} and v_{rot} : $\bar{B} \sim v_{\text{rot}}^{1.5}$.

We note that the scatter at the high- v_{rot} end in Fig. 3- top is due to the galaxies with the highest SFR, NGC 7552 and NGC 1365, as well as the Seyfert galaxy NGC 5643. The large turbulence due to high SF and AGN activities in these galaxies could enhance the generation of turbulent fields by the small-scale dynamo. It could also cause depolarization due to internal Faraday dispersion (Sokoloff et al. 1998) reducing the observed PI and S_{PI} and shifting the S_{PI}/SFR ratio to relatively low values.

5.2. Tracing the Dynamo Effect

Could the observed $\bar{B} - v_{\text{rot}}$ correlations be due to an active dynamo process? Following the linear mean-field α - Ω dynamo theory, the large-scale field is set by the shear, $S = r d\Omega/dr$, with r the galactocentric radius and Ω the angular speed. For a flat rotation curve, the shear is given by $S = -v_{\text{rot}}/r = -\Omega$. Thus, theoretically, \bar{B} can be expected to

grow proportionally with Ω , and hence the dynamo’s appropriate parameter is the angular speed and not the linear speed. However, we did not find any correlation between S_{PI}/SFR and $\Omega = v_{\text{rot}}/R_{25}^2$ (see Fig. 3- bottom).

A correlation between \bar{B} and Ω is not expected theoretically if dynamo quenching and saturation take place (Van Eck et al. 2015). This saturation occurs when the large-scale magnetic field and turbulent energy densities are similar in the interstellar medium, or because of a balance between Coriolis and Lorentz forces, or due to magnetic helicity (see Widrow et al. 2002; Van Eck et al. 2015, and references therein). In this case, the galactic large-scale dynamos are normally in a non-linear, statistically steady state. As both the quenching and growth of \bar{B} increase with Ω (Chamandy et al. 2014), a correlation between \bar{B} and Ω is not trivial in the non-linear mean-field dynamo models. Hence, \bar{B} is not expected to be correlated with either v_{rot} or Ω in these models.

The large-scale magnetic field as traced by the polarized emission could be actually dominated by an *anisotropic* turbulent field which differs from the field regulated by the dynamo process theoretically. The turbulent magnetic field could become anisotropic and apparently large-scale due to compression and/or local shear by gas streaming velocities (e.g., Laing 2011). Strong anisotropic fields in galaxies were found e.g. in M51 (Fletcher et al. 2011) and in IC342 (Beck 2015). Hence, the $\bar{B} - v_{\text{rot}}$ correlation could show that the anisotropic turbulent field dominates in faster rotating galaxies due to higher gas streaming velocities.

On the other hand, the $\bar{B} - v_{\text{rot}}$ correlation could be caused by larger \bar{B} values in galaxies with higher dynamical mass. The dynamical mass inside the optical radius is given by $M_{\text{dyn}} \approx R_{25} v_{\text{rot}}^2/G$, with G the gravitational constant. We found that S_{PI}/SFR ($\sim \bar{B}^2$)

²Averaging the actual shear in the flat part of the rotation curves results in $r \sim R_{25}$.

increases with M_{dyn} with a slope of 0.5 ± 0.1 , $\bar{B}^2 \sim M_{\text{dyn}}^{0.5 \pm 0.1}$ ($r_{\text{sp}} = 0.68 \pm 0.00$). Assuming equipartition, it follows that $\bar{B}^2 \sim M_{\text{dyn}}^{0.8 \pm 0.1}$.

Earlier attempts to establish a correlation between \bar{B} and the dynamics of galaxies met not much success, although some theoretical works went as far as suggesting an effect of \bar{B} on rotation curves of galaxies (Battaner & Florido 2007). Van Eck et al. (2015) collected the mean magnetic fields for a sample of 20 nearby galaxies. They however found no correlation between \bar{B} and v_{rot} . This, as noted by Van Eck et al. (2015), could be due to *a*) using inconsistent methods/assumptions per galaxy each referring to a different \bar{B} component and *b*) inhomogeneous galaxy sample including both interacting and isolated galaxies. We avoided these caveats by using a consistent method for all sources in our sample of the non-interacting/non-cluster galaxies.

5.3. Magnetic Energy vs Rotational Energy

The total energy of the large-scale magnetic field scales with $S_{\text{PI}}/n_{\text{cr}}$ or $S_{\text{PI}}V/N_{\text{cr}}$ (Sect. 1). Assuming $N_{\text{cr}} \sim \text{SFR}$, the magnetic energy is

$$E_{\bar{B}} \sim V S_{\text{PI}}/\text{SFR}, \quad (6)$$

while assuming equipartition leads to

$$E_{\bar{B}} \sim V S_{\text{PI}}/\text{SFR}^{0.5-0.6}. \quad (7)$$

To estimate $E_{\bar{B}}$ using Eqs. (6) and (7), the synchrotron radiating volume V is taken to be the volume of the thick disk with the radius of R_{25} and scale height of 1 kpc, corrected for inclination. The case of equipartition (Eq. (7)) even allows calibration of $E_{\bar{B}} = V \bar{B}^2/8\pi$ in ergs through

$$\bar{B} = \bar{B}_0 \frac{S_{\text{PI}}}{S_{\text{PI}_0}} \left(\frac{\text{SFR}_0}{\text{SFR}} \right)^{0.5-0.6},$$

with \bar{B}_0 , S_{PI_0} and SFR_0 the corresponding parameters of a reference galaxy. We took a galaxy residing between the dwarfs and normal spirals, i.e., M33 ($\bar{B}_0 = 2.5\mu\text{G}$, Tabatabaei et al. 2008) as the reference galaxy in the sample.

The v_{rot} data allow estimation of the rotational energy of the galaxies, $E_{\text{rot}} = \frac{1}{2}I_m\Omega^2 = \frac{1}{2}I_m(v_{\text{rot}}/R_{25})^2$, with $I_m \sim M_{\text{dyn}}R_{25}^2$ the moment of inertia. For disks, $I_m = \frac{1}{2}M_{\text{dyn}}R_{25}^2$ leading to $E_{\text{rot}} = \frac{1}{4}R_{25}^4v_{\text{rot}}^4$.

Figure. 4 shows the energy of the large-scale magnetic field $E_{\bar{B}}$ against the rotational energy of the galaxies E_{rot} . The slope of the $E_{\bar{B}} - E_{\text{rot}}$ correlation in logarithmic scale is 1.03 ± 0.10 ($r_p = 0.91 \pm 0.08$) for $N_{\text{cr}} \sim \text{SFR}$, and 1.25 ± 0.08 ($r_p = 0.96 \pm 0.06$) assuming equipartition (the magnetic-to-rotation energy changes as $2 \times 10^{-4} < E_{\bar{B}}/E_{\text{rot}} < 8 \times 10^{-2}$ with a median value of 0.002). Therefore, the two different assumptions on N_{cr} do not lead to a significant difference in the $E_{\bar{B}} - E_{\text{rot}}$ relation. These correlations show that galaxies with higher rotational energy have higher energy of the large-scale magnetic field. Considering that the rotational energy is balanced with the gravitational energy and is constant particularly for non-interacting galaxies, these relations show that the large-scale magnetic field is almost stationary at the current epoch in each galaxy (this does not reject a possibly linear dynamo process in the past). This supports the theoretical predictions that the present-day large-scale dynamos cannot be in their linear (growing) phase.

Considering active star formation as the main source of the turbulence, the $\text{SFR} - v_{\text{rot}}$ correlation implies that the turbulent energy does not change much, as long as the galaxy mass is fixed. Several studies show an equipartition between the turbulent and the *total* magnetic field energy densities (e.g., Beck 2007, 2015; Tabatabaei et al. 2008) indicating that the total magnetic field also does not evolve further.

6. SUMMARY

To study the relations between galactic magnetic fields and rotation, we selected from the literature observations of the large-scale magnetic field of galaxies which are not in clusters and are not interacting. These show a tight correlation between the polarized flux density and the rotation speed v_{rot} over three orders of magnitude in dynamical mass. Assuming $N_{\text{cr}} \sim \text{SFR}$, a linear correlation is found between the large-scale magnetic field strength \bar{B} and v_{rot} . This correlation is super-linear ($\bar{B} \sim v_{\text{rot}}^{1.5}$) assuming equipartition between the cosmic ray electrons and the total magnetic field. On the other hand, no correlation is found between \bar{B} and Ω , expected from the linear α - Ω dynamo theory. The $\bar{B} - v_{\text{rot}}$ correlation suggests that there is a coupling between the large-scale magnetic field and the dynamical mass of galaxies: $\bar{B} \sim M_{\text{dyn}}^{0.25-0.4}$. Therefore, faster rotating/ more massive galaxies have stronger magnetic fields than slower rotating/ less massive galaxies. The $\bar{B} - v_{\text{rot}}$ correlation shows that the anisotropic turbulent field dominates the large-scale field in faster rotating galaxies, perhaps due to high streaming velocities of the gas with which the magnetic field is coupled.

A comparison between the magnetic and rotational energies shows that the large-scale magnetic field is stationary and does not evolve further in galaxies with fixed dynamical mass.

This is the first study showing a statistically meaningful effect of the galaxy rotation/ mass on the large-scale magnetic fields.

We thank the anonymous referee for his/her valuable comments. We also thank Anvar Shukurov and Andrew Fletcher for stimulating discussions and to John Dickel for providing us with the LMC and SMC data. FST, TPKM, and JHK acknowledge financial support from the Spanish Ministry of Economy and Competitiveness (MINECO) under grant

number AYA2013-41243-P. JHK and JEB acknowledge financial support to the DAGAL network from the People Programme (Marie Curie Actions) of the European Unions Seventh Framework Programme FP7/2007-2013/ under REA grant agreement number PITN-GA-2011-289313.

REFERENCES

- Abrahamyan, H. V., Mickaelian, A. M., Knyazyan, A. V. 2015, *A&C*, 10, 99
- Alves, D. R., & Nelson, C. A. 2000, *ApJ*, 542, 789
- Ball, R. 1983, *BAAS*, 15, 934
- Battaner, E., & Florido, E. 2007, *Astronomische Nachrichten*, 328, 92
- Beck, R., & Hoernes, P. 1996, *Nature*, 379, 47
- Beck, R. et al. 2002, *A&A*, 391, 83
- Beck, R., Shukurov, A., Sokoloff, D., & Wielebinski, R. 2003, *A&A*, 411, 99
- Beck, R., & Wielebinski, R. 2013, *Planets, Stars and Stellar Systems Vol. 5*, by Oswalt, Terry D.; Gilmore, Gerard, ISBN 978-94-007-5611-3. Springer Science+Business Media Dordrecht, p. 641
- Beck, R. 2007, *A&A*, 470, 539
- Beck, R. 2015, *A&A*, 578, 93
- Bekki, K., & Stanimirović, S. 2009, *MNRAS*, 395, 342
- Berkhuijsen, E. M., Beck, R., & Hoernes, P. 2003, *A&A*, 398, 937
- Carignan, C., Chemin, L., Huchtmeier, W. K., & Lockman, F. J. 2006, *ApJ*, 641L, 109
- Chamandy, L., Shukurov, A., Subramanian, & K., Stoker, K. 2014, *MNRAS*, 443, 1867
- Chyży, K. T. & Buta, R. J. 2008, *ApJ*, 677, L17
- Chyży, K. T., Weżgowiec, M., Beck, R., & Bomans, D. J. 2011, *A&A*, 529, 94

- Condon, J. J. 1992, *ARA&A*, 30, 575
- Corbelli, E., & Salucci, P. 2000, *MNRAS*, 311, 441
- Cortese, L. et al., 2012, *A&A*, 544, 101
- Dickel, J. R., McIntyre, V. J., Gruendl, R. A., & Milne, D. K. 2005, *AJ*, 129, 790
- Dickel, J. R., McIntyre, V. J., Gruendl, R. A., & Milne, D. K. 2010, *AJ*, 140, 1567
- Dumke, M. & Krause, M. 1998, in *Lecture Notes in Physics*, Berlin Springer Verlag, Vol. 506, IAU Colloq. 166: The Local Bubble and Beyond, ed. D. Breitschwerdt, M. J. Freyberg, & J. Truemper, 555-558
- Dumke, M., Krause, M., & Wielebinski, R. 2000, *A&A*, 355, 512
- Fletcher, A. 2010, *ASPC*, 438, 197
- Fletcher, A., Beck, R., Shukurov, A., et al. 2011, *MNRAS*, 412, 2396
- Graeve, R. & Beck, R. 1988, *A&A*, 192, 66
- Hao, C., N. et al., 2011, *ApJ*, 741, 124
- Heesen, V., Krause, M., Beck, R., & Dettmar, R.-J. 2009, *A&A*, 506, 1123
- Heesen, V. et al. 2014, *AJ*, 147, 103
- Kennicutt, R. C. et al., 2009, *ApJ*, 703, 1672
- Kennicutt, R. C., & Evans, N. J. 2012, *ARA&A*, 50, 531
- Koribalski, B. S. et al., 2004, *AJ*, 128, 16
- Laing, R. A. 2002, *MNRAS*, 329, 417

- Lee, J. C. 2011, *ApJS*, 192, 6
- Martinsson, T. P. K. et al., 2015, arXiv151007666M
- Massardi, M. et al., 2013, *MNRAS*, 436, 2915
- Mateo, M. L. 1998, *ARA&A*, 36, 435
- Murphy, E. J., Helou, G., Kenney et al., 2008, *ApJ*, 678, 828
- Sofue, Y. et al. 1999, *ApJ*, 523, 136
- Sofue, Y., Tuti, Y., Honma, M., & Tomita, A. 1997, *AJ*, 114, 2428
- Sokoloff, D. D. et al., 1998, *MNRAS*, 299, 189
- Sparre, M., et al. 2015, *MNRAS*, 447, 3548
- Steenbeck, M., Krause, F. 1969, *AN*, 291, 271
- Tabatabaei, F. S., Krause, M., & Beck, R. 2007, *A&A*, 472, 785
- Tabatabaei, F. S., Krause, M., Fletcher, A., & Beck, R. 2008, *A&A*, 490, 1005
- Tabatabaei, F. S., Schinnerer, E., Murphy, E. J. et al. 2013, *A&A*, 552, 19
- Tabatabaei, F. S., Berkhuijsen, E., M., Frick, P. et al. 2013, *A&A*, 557, 129
- Tully, R., B., & Fisher, J., R. 1977, *A&A*, 54, 661
- Van Eck, C. L., Brown, J. C., Shukurov, A., & Fletcher, A. 2015, *ApJ*, 799, 35
- Widrow, L. M. 2002, *Reviews of Modern Physics*, 74, 775

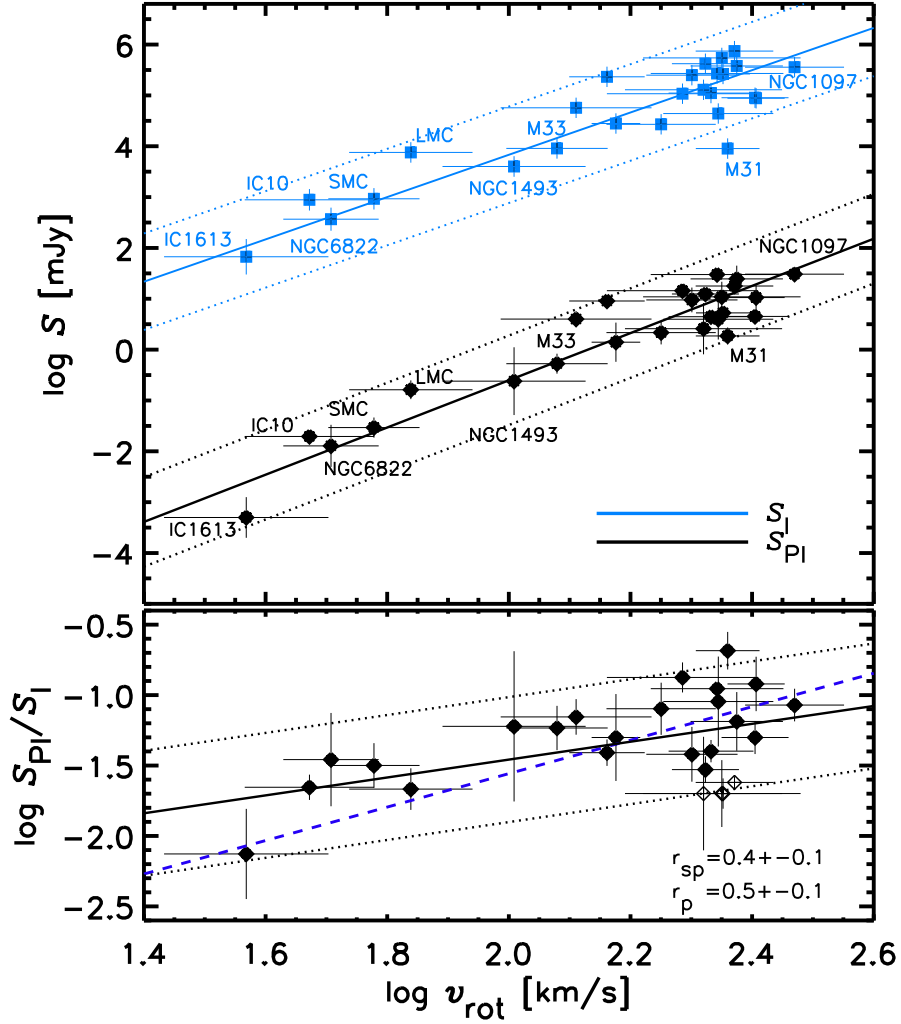


Fig. 1.— *Top*: integrated total (top, blue squares) and polarized flux densities (bottom, black dots) projected at a distance of 10 Mpc vs. the rotation speed of galaxies, v_{rot} . *Bottom*: fractional polarization S_{PI}/S_I against v_{rot} . The lines show the least square fits (solid) and their 2σ scatter (dotted). In the bottom panel, the dashed line shows the bisector fit and open symbols indicate NGC 7552, NGC 1365, NGC 5643 (Sect. 5.1).

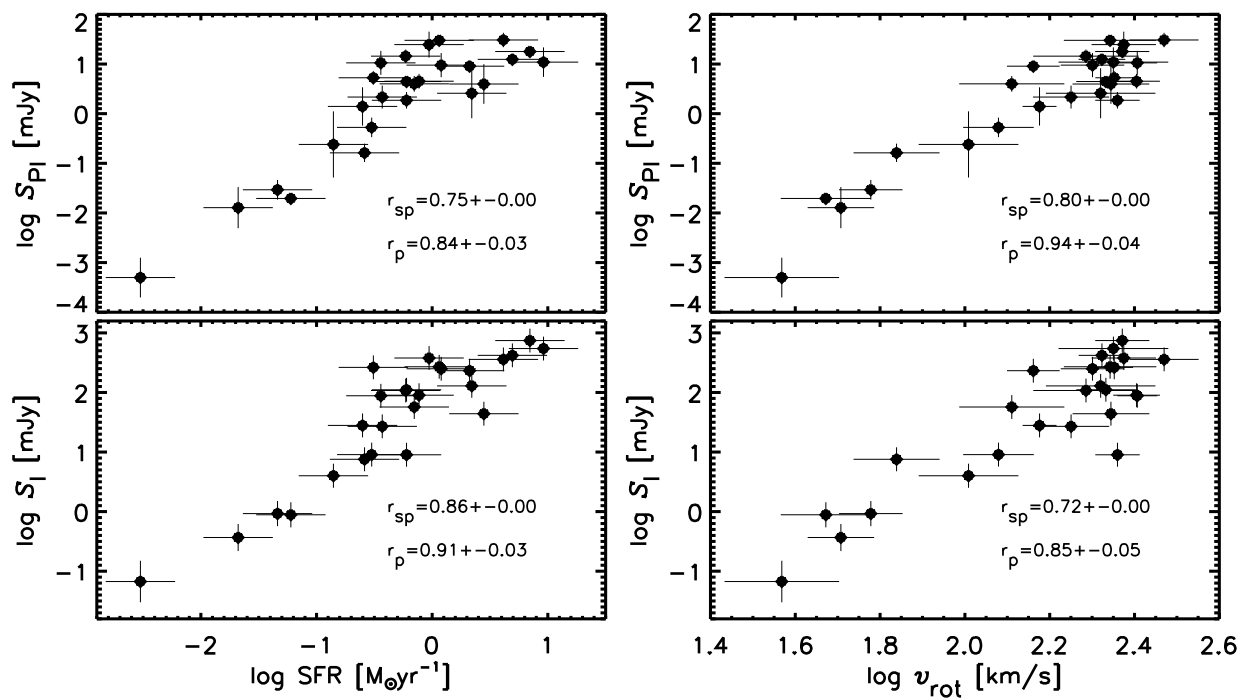


Fig. 2.— Integrated polarized (S_{PI} , top) and total flux densities (S_I , bottom) against SFR (left panels). The horizontal error bars show a 25% uncertainty. Shown for comparison are S_{PI} and S_I against v_{rot} (right panels).

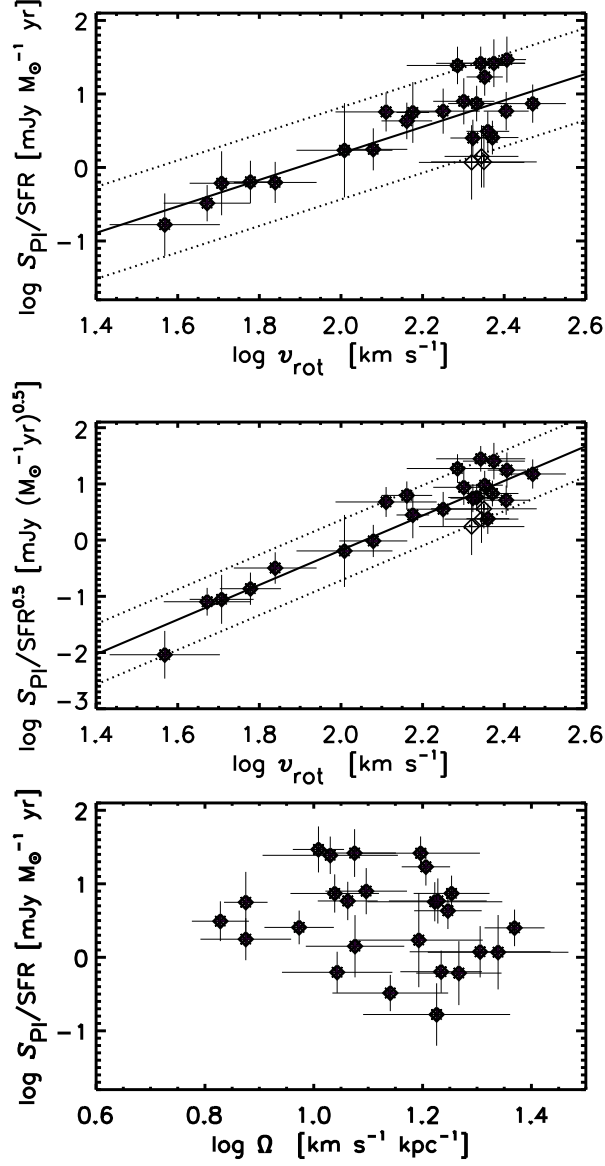


Fig. 3.— *Top*: ratio of the integrated polarized flux density to the SFR vs. the rotation speed. *Middle*: ratio of the integrated polarized flux density to the $\text{SFR}^{0.5}$ vs. the rotation speed. Open symbols indicate NGC 7552, NGC 1365, and NGC 5643 (see text). *Bottom*: ratio of the integrated polarized flux density to the SFR vs. the angular speed.

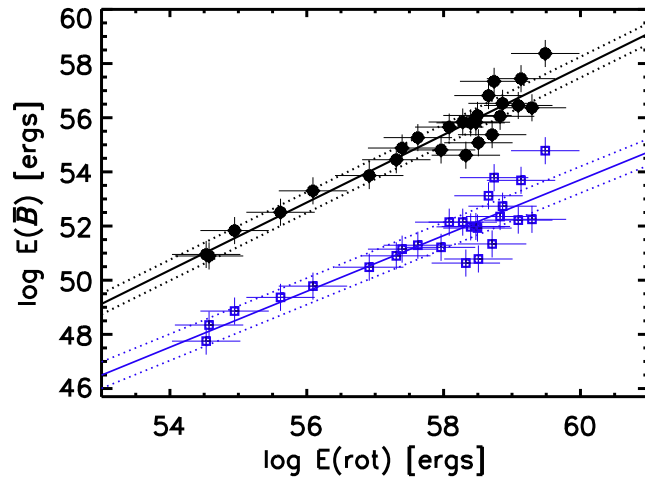


Fig. 4.— Energy of the large-scale magnetic field $E(\bar{B})$ vs. the rotational energy $E(\text{rot})$ in ergs assuming equipartition (dots). Squares show $E(\bar{B})$ in arbitrary units vs. $E(\text{rot})$ assuming $N_{\text{cr}} \sim \text{SFR}$. The lines show the ordinary least square fits (solid) and their 5σ scatter (dotted). The error bars indicate a 50% uncertainty.

Table 1. Properties of the galaxy sample.

Galaxy Name	Hubble Type	Inclination [$^{\circ}$]	Distance [Mpc]	S_{I} [mJy]	S_{PI} [mJy]	v_{rot} [km/s]	R_{min} [kpc]	R_{max} [kpc]	SFR [M_{\odot}/yr]	R_{25} [kpc]
IC342	SABcd	25	3.1	108 ± 9^1	14 ± 2^1	$193 \pm 24^{\text{S}}$	5	18	0.59	11.87
NGC6946	SABcd	30	6.8	270 ± 55^2	30 ± 1.1^2	$220 \pm 24^{\text{S}}$	6	14	1.15	9.18
NGC253	SABc	78	3.94	420 ± 25^4	12.4 ± 1.5^4	$211 \pm 12^{\text{S}}$	2	9	4.94	13.77
NGC3628	SAB pec	86	6.7	111 ± 20^5	4.4 ± 0.4^5	$215 \pm 15^{\text{S}}$	2	12	0.6	18.34
NGC4565	SAb	86	13.1	88 ± 10^5	10.6 ± 2.5^5	$255 \pm 12^{\text{S}}$	5	25	0.36	62.61
NGC4736	SABab	35	4.7	27 ± 6^6	2.16 ± 0.50^6	$178 \pm 16^{\text{S}}$	3	7	0.37	7.91
NGC5907	Sc	88	16.4	90 ± 7^7	4.5 ± 0.7^7	$254 \pm 14^{\text{S}}$	5	22	0.77	28.14
NGC891	SAb	88	8.4	264 ± 45^5	5.3 ± 0.7^5	$225 \pm 10^{\text{S}}$	4	14	0.31	18.48
NGC1097	SBbc	40	16	359 ± 30^3	30.5 ± 4.4^3	$295 \pm 24^{\text{S}}$	5	27	4.13	22.35
NGC1365	SBb	46	19	744 ± 47^3	17.9 ± 0.9^3	$235 \pm 15^{\text{S}}$	15	25	7	35.01
NGC3359	SBc	51	11	28 ± 2^3	1.4 ± 0.8^3	$149 \pm 6^{\text{BA}}$	11	20	0.25	20.65
NGC1493	SBc	27	12	4 ± 1^3	0.24 ± 0.16^3	$102 \pm 12^{\text{W}}$	0.14	6.54
NGC1559	SBc	57	15	232 ± 13^3	9.1 ± 1.1^3	$145 \pm 9^{\text{W}}$	2.1	8.22
NGC1672	SBb	39	15	250 ± 14^3	9.5 ± 2.3^3	$200 \pm 15^{\text{W}}$	1.2	16.02
NGC3059	SBc	27	14	57 ± 4^3	3.99 ± 0.63^3	$129 \pm 16^{\text{W}}$	0.7	7.73
NGC5643	SBc	23	14	129 ± 8^3	2.6 ± 1.3^3	$209 \pm 27^{\text{W}}$	2.2	9.58
NGC7552	SBbc	28	21	546 ± 87^3	10.9 ± 3.2^3	$224 \pm 29^{\text{W}}$	9.2	11.08
NGC1300	SBb	35	20	44 ± 8^3	3.96 ± 1.58^3	$221 \pm 20^{\text{W}}$	2.8	18.56
NGC7479	SBbc	45	34	379 ± 46^3	24.6 ± 6.4^3	$237 \pm 18^{\text{W}}$	0.9	19.94
M31	SAb	77	0.69	9 ± 1^8	1.9 ± 0.3^8	$229 \pm 12^{\text{C}}$	16	34	0.6	21.06
M33	SACd	54	0.84	9.06 ± 0.95^9	0.53 ± 0.1^9	$120 \pm 10^{\text{CS}}$	0.30	8.49
LMC	Irr/SBm	33	0.050	7.6 ± 1.5^{10}	0.16 ± 0.03^{10}	$69 \pm 7^{\text{A}}$	2.5	13	0.26	4.70
SMC	Irr	40	0.060	0.9 ± 0.2^{11}	0.029 ± 0.006^{11}	$59 \pm 4.5^{\text{B}}$	0.046	2.75

Table 1—Continued

Galaxy Name	Hubble Type	Inclination [°]	Distance [Mpc]	S_{I} [mJy]	S_{PI} [mJy]	v_{rot} [km/s]	R_{min} [kpc]	R_{max} [kpc]	SFR [M_{\odot}/yr]	R_{25} [kpc]
IC10	Irr	40	0.66	0.88 ± 0.15^{12}	0.020 ± 0.002^{12}	$47 \pm 5^{\text{M}}$	2.68	3.40	0.06	0.60
NGC6822	Irr	67	0.50	0.37 ± 0.07^{12}	0.013 ± 0.005^{12}	$51 \pm 4^{\text{M}}$	0.02	1.13
IC1613	Irr	35	0.73	0.07 ± 0.01^{12}	0.0005 ± 0.0002^{12}	$37 \pm 5^{\text{M}}$	0.003	1.72

Note. — The integrated flux densities S_{I} and S_{PI} were measured at 4.8 GHz and projected to a distance of 10 Mpc. The Hubble type and distance are taken from the NASA Extragalactic Database, 1- Graeve & Beck (1988), 2- Beck & Hoernes (1996), 3- Beck et al. (2002), 4- Heesen et al. (2009), 5- Dumke & Krause et al. (1998), 6- Chyży & Buta (2008), 7- Dumke et al. (2000), 8- Berkhuijsen et al. (2003), 9- Tabatabaei et al. (2007, 2008), 10- Dickel et al. (2005), 11- Dickel et al. (2010), 12- Chyży et al. (2011), A- Alves & Nelson (2000), B- Bekki & Stanimirović (2009), BA- Ball (1983), C- Carignan et al. (2006), CS- Corbelli & Salucci (2000), M- Mateo (1998), S- Sofue et al. (1999), W- Koribalski et al. (2004). The inclinations were taken from the v_{rot} references.